Asymmetric exclusion process in a system of interacting Brownian particles

José Eduardo de Oliveira Rodrigues* and Ronald Dickman†
Departamento de Física, ICEx, Universidade Federal de Minas Gerais, Caixa Postal 702, Belo Horizonte, MG 30161-970, Brazil
(Received 1 February 2010; revised manuscript received 23 April 2010; published 4 June 2010)

We study a continuous-space version of the totally asymmetric simple exclusion process (TASEP), consisting of interacting Brownian particles subject to a driving force in a periodic array of potential wells. Particles are inserted into the leftmost well at rate α, hop to the right at unit rate, and are removed at the rightmost well at rate β. Our study is motivated by recent experiments on colloidal particles in a periodic potential generated by an optical tweezers array. Particles spend most of the time near potential minima, approximating the situation on the lattice; a short-range repulsive interaction prevents two particles from occupying the same potential well. A constant driving force, representing Stokes drag on particles suspended in a moving fluid, leads to biased motion. Our results for the density profile and current, obtained via numerical integration of the Langevin equation and dynamic Monte Carlo simulations, indicate that the continuous-space model exhibits phase transitions analogous to those observed in the lattice TASEP. The correspondence is not exact, however, due to the lack of particle-hole symmetry in our model.

DOI: 10.1103/PhysRevE.81.061108 PACS number(s): 02.50.Ey, 05.70.Fh, 05.60.Cd

I. INTRODUCTION

A driven lattice gas, or a driven diffusive system, is a collection of interacting particles that hop in a preferred direction on a lattice. The system cannot reach equilibrium but may attain a stationary state with a steady current; the model is a prototype for studies of nonequilibrium states [1–4]. The simplest example of a driven diffusive system, which has become one of the standard models of nonequilibrium statistical mechanics, is the totally asymmetric simple exclusion process (TASEP) [5–8]. In the TASEP with open boundaries the edge sites are connected to particle reservoirs with fixed densities. Introduced as a model of biopolymerization [9] and transport across membranes [10], over the years, this model has been applied to other processes, e.g., traffic flow [11] and cellular transport [12,13].

From a mathematical point of view the model is of interest in the theory of interacting particle systems since, despite its simplicity, it shows a nontrivial behavior [7,8,14,15]. In the one-dimensional TASEP with open boundaries, particles jump only to the right, along a one-dimensional lattice whose sites can be empty or occupied by a single particle. Particles are injected at the leftmost site at rate α if this site is empty and are removed at the rightmost site at rate β if this site is occupied. The one-dimensional TASEP, which has been solved exactly, exhibits three distinct phases in the α-β plane [16–19]. The phase transition is discontinuous along the line $\alpha=\beta<1/2$, where the density profile is linear, and is continuous along the lines $\alpha=1/2$, $\alpha>\beta$ and $\beta=1/2$, $\alpha<\beta$ (see Fig. 9). Although this model and variants have been the subject of intensive theoretical study, there is as yet no realization of a TASEP-like system in the laboratory.

The invention of optical tweezers arrays has made possible experimental studies of the dynamics of colloidal particles in a periodic external potential [20–25]. The motion at long times and low friction consists of jumps between adjacent potential minima. If the particle and potential well sizes are chosen properly, only one particle can occupy a given well. The exclusion process is a caricature of this dynamics, suggesting that a system of colloidal particles in an optical tweezers array could be designed as a laboratory realization of the TASEP. Motivated by this possibility, we propose a model in continuous space having the same essential characteristics as the lattice TASEP. Our model represents colloidal particles immersed in a fluid flowing at constant rate through a one-dimensional optical tweezers array, restricting particle motion to the array axis. Specifically, we study a one-dimensional system of interacting Brownian particles subject to a periodic external potential and to a constant external force representing the drag due to the fluid motion. A short-range (essentially hard-sphere) repulsion between particles prevents more than one particle occupying the same potential well. This continuous-space model is studied via numerical integration of the Langevin equation and dynamic Monte Carlo (MC) simulation. We observe phase transitions analogous to those found in the lattice TASEP. Some differences in the detailed behavior nevertheless appear due to the lack of particle-hole symmetry in the continuous-space model. Details on the model and simulation methods are given in Secs. II and III. Simulation results are presented in Sec. IV, while our conclusions and prospects for future work are outlined in Sec. V.

II. CONTINUOUS-SPACE MODEL

Our aim is to study a continuous-space model sharing the same essential features as the TASEP (defined on a lattice) as a step toward experimental realization of a TASEP-like system. The model should possess the following characteristics: (i) confinement of particles to a one-dimensional structure, (ii) localization of particles at potential minima ("wells") of a linear periodic array with (iii) multiple occupancy prohibited, (iv) biased hopping between adjacent wells, and (v) insertion (removal) of particles at the initial (final) well. Cri-

*jeo@fisica.ufmg.br
†dickman@fisica.ufmg.br

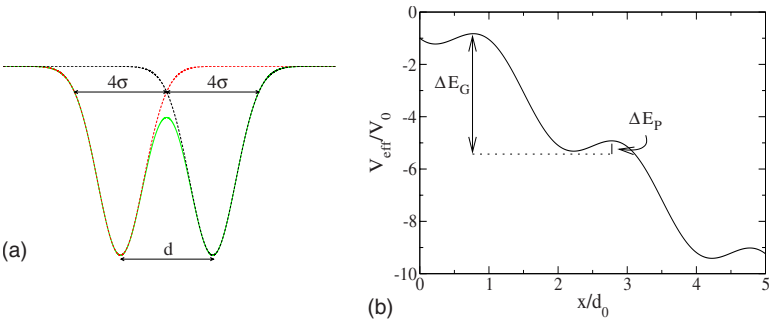

FIG. 1. (Color online) (a) Two neighboring Gaussian profiles (red and black dotted curves) and their sum (green solid curve); (b) effective external potential.

teria (i)–(iii) are realizable with a suitably tailored optical tweezers array. The array consists of a series of spherically symmetric optical tweezers; the particles flow along this line, which we take as the x axis. To avoid particles escaping the array, there should be a substantial overlap between neighboring wells, so that a potential maximum at a point midway between two wells is in fact a saddle point in the full three-dimensional space [see Fig. 1(a)]. For a TASEP-like system, it is crucial that the probability of a particle escaping from the array is negligible on the time scale of the experiment. Effective confinement requires that the potential barrier to escape the array be much larger than k_BT; the barrier between adjacent minima should be $\sim k_BT$ to allow transitions between neighboring wells. In what follows we shall assume that this condition is satisfied and consider, for simplicity, a one-dimensional system. Fluctuations of the particle positions in the directions perpendicular to the array will therefore be ignored, but should be included in a more complete analysis.

The diameter of the optical tweezers well should be slightly greater than the particle diameter, so that at most one particle can occupy the well at a given time. Due to thermal fluctuations, particles will occasionally overcome the potential barrier separating neighboring wells. Since hopping must be asymmetric, we impose a steady fluid motion along the $+x$ axis, which effectively prohibits particle jumps in the opposite direction. In the lattice TASEP particles are inserted in the first site and removed from the last. Experimental realization of this feature is subtler, but can in principle be achieved using optical tweezers to drag particles into the first well, and out of the last one, at prescribed rates. We discuss an alternative method of insertion and removal in Sec. V.

The above sketch of an experimental setup motivates our study of Brownian motion of interacting colloidal particles in an optical tweezers array. The Langevin equation for the ith particle is

$$m\ddot{x}_i(t) = -b[\dot{x}_i(t) - v] - \frac{\partial V_{ext}(x_i)}{\partial x_i} - \frac{\partial}{\partial x_i}[V_{int}(x_{i,i-1}) + V_{int}(x_{i,i+1})] + m\Gamma_i(t), \quad (1)$$

where x_i, $\dot{x}_i$, and $\ddot{x}_i$ are, respectively, the position, velocity, and acceleration of particle i; $x_{i,j} \equiv x_j - x_i$; v is the fluid velocity; and V_{ext} is the periodic external potential. V_{int} is the (strongly repulsive) interparticle potential. (We assume the range of V_{int} to be short enough such that only neighboring particles interact.) The first term on the right side of Eq. (1) represents damping of the particle velocity relative to the fluid. For a sphere of radius R, Stokes law gives

$$b = 6\pi\mu R, \quad (2)$$

where μ is the fluid viscosity. Here, it is important to stress that the fluid is three dimensional although we treat the particle motion as one dimensional. The final term is a random noise with the following properties:

$$\langle \Gamma_i \rangle = 0, \quad (3)$$

$$\langle \Gamma_i(t)\Gamma_j(t') \rangle = \frac{2bk_BT}{m^2}\delta_{i,j}\delta(t-t'), \quad (4)$$

where $k_B = 1.380\,650\,4 \times 10^{-23}$ J/K is the Boltzmann constant, T is temperature, and m is the particle mass. It is convenient to ignore the inertial term $m\ddot{x}_i(t)$ in Eq. (1) since the observational times of interest (microseconds or greater) are much larger than the relaxation time of the velocity, $m/b \sim 10^{-8}$ s, for our choice of parameters. Then the velocity of particle i follows

$$\dot{x}_i(t) = v - \frac{1}{b}\frac{\partial V_{ext}(x_i)}{\partial x_i} - \frac{1}{b}\frac{\partial}{\partial x_i}[V_{int}(x_{i,i-1}) + V_{int}(x_{i,i+1})] + \frac{m}{b}\Gamma_i(t). \quad (5)$$

A. Potentials

The potential of an optical tweezers array can be represented by a sum of n identical Gaussian profiles of width σ and spatial period d,

$$V_t(x) = -V_0 \sum_{n=0}^{N} e^{-(x-dn)^2/2\sigma^2}. \quad (6)$$

We require neighboring wells to overlap, which can be accomplished by setting $\sigma \lesssim d$; Fig. 1(a) shows that this condition is satisfied for $\sigma = d/4$. For this choice of parameters, the potential is well approximated by a cosine as can be seen from the Fourier coefficients

$$a_n = \frac{2}{d}\int_0^d \cos\left(\frac{2n\pi x}{d}\right)\left[-\sum_{n=0}^{N} e^{-(x-dn)^2/2\sigma^2}\right]dx. \quad (7)$$

Numerical evaluation yields

$$a_0 = -0.627,$$

$$a_1 = 0.365,$$

$$a_2 = 9.010 \times 10^{-3}. \tag{8}$$

Note that $a_2/a_1 \simeq 0.025$, allowing us to write, to a good approximation, the array potential as a constant plus a cosine term. For the one-dimensional model studied here, we define

$$V_{ext}(x) = -V_0 \cos\left(\pi \frac{x}{d_0}\right) \tag{9}$$

as the periodic external potential. The interaction between colloidal particles is taken as purely repulsive; for convenience we use a truncated $1/r^{12}$ potential,

$$V_{int}(r) = \begin{cases} U_0\left[\left(\frac{a}{r}\right)^{12} - 1\right], & r \le a \\ 0, & r \ge a, \end{cases} \tag{10}$$

where a is the particle diameter and r is the distance between neighboring particles.

B. Parameter values

To specify the external and interaction potentials, we need to fix V_0 and U_0. These values must be chosen so as to approximate the TASEP dynamics given the length, time, and energy scales characterizing the system. We measure lengths in units of microns, time in seconds, and energies in units of $k_BT = 4.141\,951\,2 \times 10^{-21}$ J, assuming a temperature of 300 K. We set $d_0 = 1$ (so that the period of the external potential is 2 μm) and take the particle diameter as $a = 1.8$, so that a pair of particles occupying neighboring wells have some freedom to fluctuate about the potential minima. Taking the fluid as water [with viscosity $\mu = 0.01$ g/(cm s)] we fix the friction coefficient as $b \cong 1.697 \times 10^{-8}$ J s/m^2 or $b \cong 4.096 k_BT$ s/μm^2 in our units.

To determine the fluid velocity v and external-potential intensity V_0 we examine the effective external potential, defined as

$$V_{eff} = -V_0 \cos\left(\pi \frac{x}{d_0}\right) - bvx, \tag{11}$$

i.e., the sum of external periodic potential and a fictitious potential representing the constant friction force acting on particles [see Fig. 1(b)]. If $bvd_0 \gg V_0$, particles do not feel the periodic potential, while if $bvd_0 \ll V_0$ particle hopping is essentially unbiased. Let ΔE_G (ΔE_P) denote the difference between a given maximum of V_{eff} and the first minimum to the right (left) of this maximum. In this way, ΔE_G (ΔE_P) is the potential barrier separating a given potential minimum from its left (right) neighbor. A simple calculation shows that

$$\Delta E_G - \Delta E_P = 2bvd_0,$$

$$\Delta E_G + \Delta E_P = 4V_0 \cos(\pi x_0/d_0) + 4bvx_0, \tag{12}$$

with

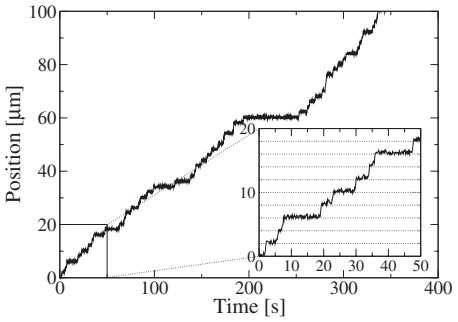

FIG. 2. A typical single-particle trajectory.

$$x_0 = \frac{d_0}{\pi} \sin^{-1}\left(\frac{bvd_0}{\pi V_0}\right), \tag{13}$$

such that the potential minima occur at $x_j = 2jd_0 + x_0$ and maxima at $y_j = 2jd_0 + 1 - x_0$ for j an integer. Given ΔE_G and ΔE_P, we can determine x_0, v, and V_0. We take $\Delta E_P \sim k_BT$, and $\Delta E_G \gg k_BT$, so that a particle has a finite rate of jumping to the well on the right and virtually has no chance of jumping in the opposite direction. We show in the following section that this condition is satisfied for $\Delta E_G = 20 k_BT$ and $\Delta E_P = 2k_BT$. For these values we have

$$v = 2.1974 \ \mu\text{m/s},$$

$$V_0 = 4.5680 k_BT,$$

$$x_0 = 0.215 \ \mu\text{m}. \tag{14}$$

To maintain the interparticle repulsion in the presence of the external potential, we must take U_0 substantially greater than V_0. On the other hand, very large values of U_0 are inconvenient for numerical integration of the Langevin equation, as a very small time increment would be required to avoid spurious particle displacements. We therefore use $U_0 = 40 k_BT \simeq 9V_0$.

C. Single-particle dynamics

To begin, we study the motion of a single Brownian particle in the system defined above. Figure 2 shows a representative time series of the particle position; the sizes of the plateaux correspond to the times spent in a given well. Using time series of this kind, we determine the mean transition time τ between neighboring wells to be 6.5380(9) s. This quantity is needed in order to define the insertion and removal rates. (Recall that in the lattice TASEP these rates are defined in units of the hopping rate.) If the first well is empty we insert a particle there (at the potential minimum position), at rate α/τ; if the last well is occupied, we remove the particle at rate β/τ.

III. DYNAMIC MONTE CARLO SIMULATIONS

The Langevin simulation (LS) outlined in the preceding section is valuable for fixing the time scale of hopping between wells and for confirming the basic phenomenology of the model. It is, however, rather inefficient numerically, so

that it is desirable to implement a dynamic MC simulation for large-scale studies. We apply the Metropolis algorithm to evolve the particle positions in time.

In this approach we use the following expression for the potential energy:

$$E = -\sum_{i=1}^{N} [V_0 \cos(\pi x_i) + bvx_i] + \sum_{i=1}^{N-1} V_{int}(x_{i+1} - x_i), \quad (15)$$

where V_{int} is given by Eq. (10). The drag force due to the moving fluid is represented by the effective potential $-bvx$. In the MC dynamics, a trial configuration is generated by selecting one of the N particles at random and subjecting it to a random displacement Δx, chosen from a Gaussian distribution with mean zero and standard deviation $\sigma=0.2$ μm. This value is 10% of the well size, large enough to afford a substantial speedup, but small enough that the probability of a particle displacement greater than 2 μm is negligible. As is usual in Metropolis MC, trial moves such that the change in energy $\Delta E \leq 0$ are always accepted, while for $\Delta E > 0$ the trial move is accepted with probability $e^{-\Delta E/k_B T}$. We determine the mean number of Monte Carlo steps required for a particle move from one well to its neighbor on the right as $N_{MC}=120.917(1)$. Thus, the time per Monte Carlo step is

$$\tau_0 = \frac{\tau}{N_{MC}} = 5.4070(8) \times 10^{-2} \text{ s}. \quad (16)$$

Particle insertion and removal are done as in the Langevin simulations. We verify below that this method is equivalent to the latter approach; the MC algorithm is ~1000 faster than numerical integration of the Langevin equation, for $L=100$.

IV. RESULTS

During the simulations we monitor the mean occupation probability $\rho(i)$ at each well i, and the current J, given by the mean number of particles leaving the system per unit time. Examples of density profiles in the stationary regime [$\rho(i)$ versus i] are shown in Fig. 3 for several values of α, with $\beta=0.4$. (From here on α and β are given in units of $1/\tau$, where τ is the mean time required for hopping between wells.) This figure shows that the continuous-space model exhibits the same basic phenomenology as the lattice TASEP. For $\alpha \leq 0.4$ the overall density grows with α. On increasing α from 0.4 to 0.5 there is a marked increase in density, but for further increases the density changes very little. While the LS results already suggest that the model exhibits phase transitions, we shall use the more precise results of our MC simulations to perform a detailed analysis. Before proceeding, we verify that the MC method yields results in agreement with the LS. In Fig. 4 we compare density profiles obtained via LS and MC for the same values of α and β. The bulk densities obtained using the two methods differ by $\leq 1.6\%$. Thus, the MC method captures the behavior found using the Langevin equation to good precision.

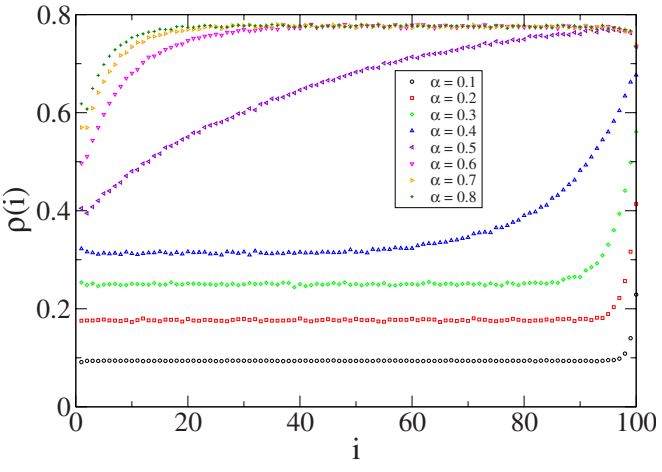

FIG. 3. (Color online) Density profile for $\beta=0.4$ obtained via numerical integration of the Langevin equation, for α values as indicated; $L=100$.

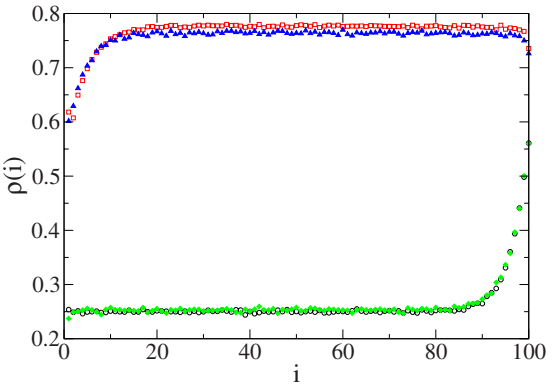

FIG. 4. (Color online) Comparison between profiles obtained using LS (open symbols) and MC (filled symbols), $\alpha=0.3$ (lower curves), $\alpha=0.8$ (upper curves), $\beta=0.4$, and $L=100$.

We perform MC simulations of systems of $L=100$, 200, and 500 wells. Far from the phase transition, density profiles depend only weakly on the system size, but near the transition there are significant finite-size effects, as illustrated in Fig. 5. In this case, as L increases, the profile tends to a near-constant value except for a sharp increase near the exit.

To minimize boundary effects we study the *bulk* density ρ, defined as the mean density over the 10% of sites nearest the center,

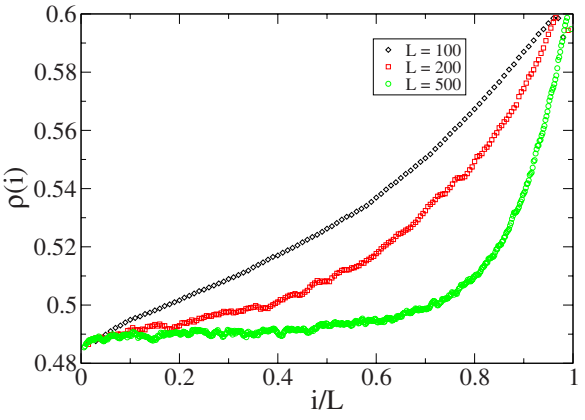

FIG. 5. (Color online) Density profiles for $\alpha=0.7$ and $\beta=0.6$, for systems of 100, 200, and 500 wells.

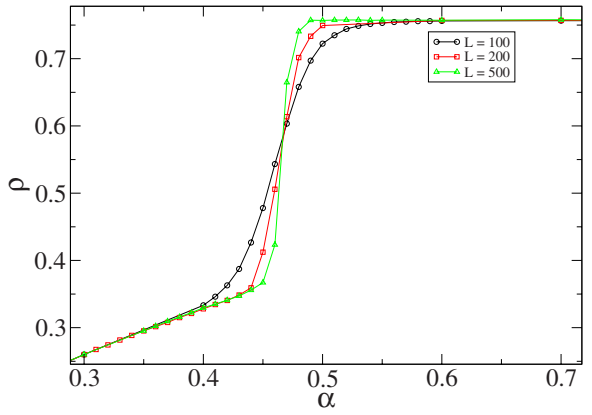

FIG. 6. (Color online) Bulk density versus α for $\beta=0.4$; system sizes $L=100$, 200, and 500.

$$\rho = \frac{10}{L} \sum_{i=0.46L}^{0.55L} \rho(i). \tag{17}$$

The bulk density as a function of α, for $\beta=0.4$, is shown in Fig. 6 for the three system sizes studied. These results strongly suggest the development of a discontinuity in $\rho(\alpha)$ near $\alpha=0.47$ as the system size is increased.

A. Phase diagram

Before determining the phase diagram in detail, we note that Fig. 7, which provides an overview of how the bulk density and the current depend on the control parameters, shows evidence of both continuous and discontinuous phase transitions. For $\alpha<0.8$ or so, and $\beta<\alpha$, the system is in the high-density phase since the density and current depend only on β, whereas for $\beta>\alpha$, and $\beta<0.6$ or so, the system is in the low-density phase, in which ρ and J depend only on α. For larger values ($\alpha>0.8$ and $\beta>0.6$), the system is in the maximum-current phase, in which ρ and J are independent of both α and β, and J takes its maximum value. Thus, the continuous-space model exhibits the same three phases observed in the lattice model. As in the lattice model, the transition between the low- and high-density phases is discontinuous, whereas transitions between the maximum-current phase and the other phases are continuous. (While the density is discontinuous in the former case, the current is always continuous at the transition.)

Kolomeisky *et al.* [26] showed how the phase diagram of a TASEP-like system (with open boundaries) can be determined from the current-density relation $J(\rho)$ for the corresponding system with periodic boundaries, assuming that $J(\rho)$ possesses a single maximum, J_{max}, at the density ρ^*. Suppose that the leftmost site is connected to a reservoir with

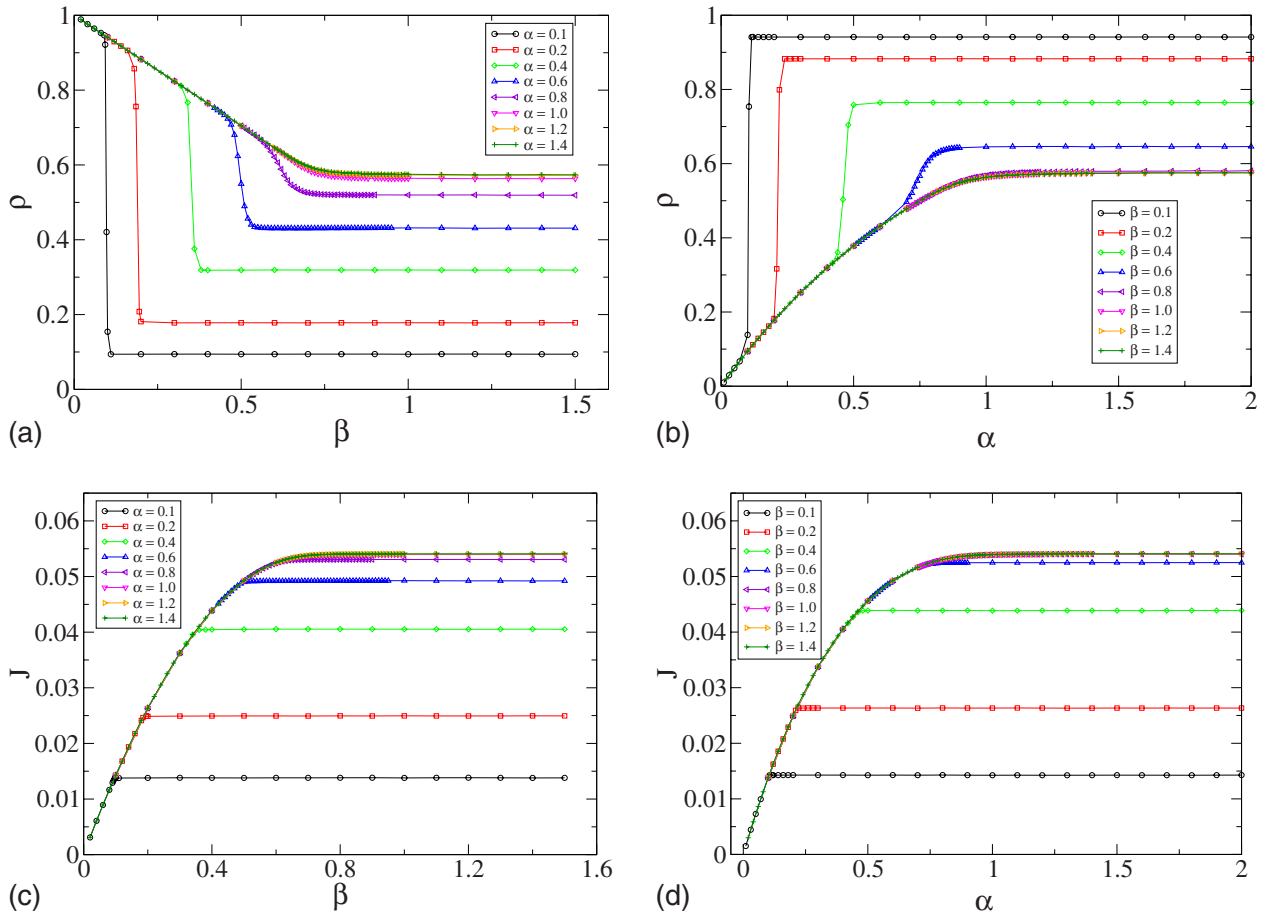

FIG. 7. (Color online) Upper panels: bulk density for (a) fixed α and (b) fixed β. Lower panels: current for (c) fixed α and (d) fixed β. System size $L=200$.

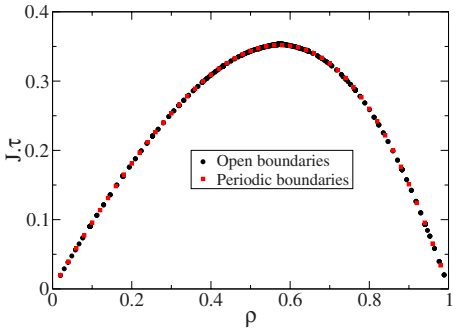

FIG. 8. (Color online) Current versus density for $L=200$ with open and periodic boundary conditions.

density ρ_-, and the rightmost site is connected to a reservoir with a higher density ρ_+. The coexistence line between the low- and high-density phases is given by $J(\rho_-)=J(\rho_+)<J_{max}$. In the low-density phase $[J(\rho_-)<J(\rho_+)]$ the bulk density $\rho=\rho_-<\rho^*$, while in the high-density phase $[J(\rho_-)>J(\rho_+)]$ the bulk density $\rho=\rho_+>\rho^*$. The continuous transition lines are $\rho_-=\rho^*$ for $\rho_+<\rho^*$ and $\rho_+=\rho^*$ for $\rho_->\rho^*$.

The above observations allow one to find the transition lines once $J(\rho)$ is known. Simulations with open boundaries furnish $J(\bar{\rho})$ with $\bar{\rho}$ given by Eq. (17). These data, however, are not convenient for the analysis since the density values are not equally spaced and, moreover, the bulk density values given by Eq. (17) have statistical uncertainties. We therefore perform MC simulations on a ring of $L=200$ wells (in continuous space) to obtain $J(\rho)$ at equally spaced fixed particle densities, $\rho=N/L$. Figure 8 shows that the current-density relations obtained using open and periodic boundaries are in excellent agreement. For subsequent analysis, we fit an eighth-degree polynomial to $J(\rho)/[\rho(1-\rho)]$, using the data obtained with periodic boundaries. (We fit $J/[\rho(1-\rho)]$, rather than J itself, to guarantee that the resulting expression for the current vanishes at $\rho=0$ and $\rho=1$.) Using the polynomial fit, we find $\rho^*=0.575\,489(3)$ [the uncertainty in ρ^* reflects that in $J(\rho)$]. The coexisting densities, ρ_+ and ρ_-, along the discontinuous transition curve, are determined using $J(\rho_-)=J(\rho_+)$ [26].

It remains to determine the phase diagram in the α-β plane, a task that cannot be accomplished solely on the basis of the function $J(\rho)$ since, off lattice, the relation between the rates α and β, and the bulk density ρ is nontrivial and not known *a priori*. Therefore, using the data from simulations with *open* boundaries, we equate ρ_- to the bulk density $\rho_L(\alpha)$ in the low-density phase and equate ρ_+ to the bulk density $\rho_H(\beta)$ in the high-density phase. [The bulk densities ρ_L and ρ_H are determined in simulations using $\beta=1.6$ and $\alpha=2.0$, respectively; see Figs. 7(b) and 7(a).] Inverting these relations (numerically, using polynomial fits), each point in the ρ_+-ρ_- plane is mapped to a point in the α-β plane.

The above procedure, making use of the current-density relation for the periodic system, is expected to provide the most reliable results for the phase diagram [26]. We refer to this as "method A." For comparison, we estimate the phase diagram using the results of simulations with open boundaries ("method B"). Here, we use polynomial fits to the data for the current as a function of the rates α and β (see Fig. 7)

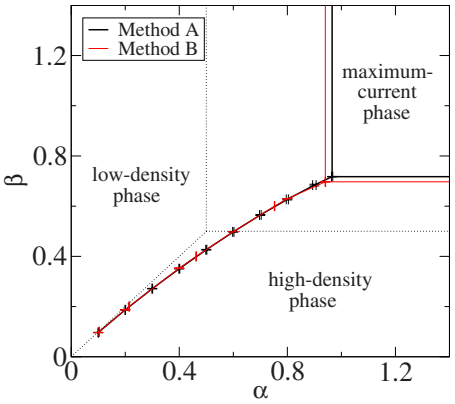

FIG. 9. (Color online) Phase diagram of the TASEP on the lattice (dotted lines) and in continuous space (solid lines) for $L=200$ obtained using methods A and B described in the text.

to estimate the transition points. Consider first the case of fixed α. For small β, the stationary current depends only on β [see Fig. 7(c)]. We therefore fit a polynomial $P(\beta)$ to the current in the regime $\beta<0.6$, using data for a large fixed α ($\alpha=2.0$). For larger values of β, the current depends only on α; in Fig. 7(c) this regime corresponds to one of the plateaux, $J=J^*(\alpha)$. The transition point $\beta_c(\alpha)$ is taken as the value at which the plateau intersects the polynomial fit to the small-β data, i.e., $P(\beta_c)=J^*(\alpha)$. Determination of $\alpha_c(\beta)$ follows an analogous procedure, in which we fit a polynomial to the current data for $\alpha<0.85$. We find that a quadratic polynomial is sufficient to fit (to within uncertainty) the current $J(\beta)$ at fixed α, while a good fit of $J(\alpha)$ (at fixed β) requires a quartic polynomial. We determine points along the continuous transition lines via the criterion that the current attains its maximum value at the transition.

Using the methods described above we construct a phase diagram based on the data for each system size studied; that for $L=200$ is shown in Fig. 9. We verified that the boundaries for $L=100$ and 500 are nearly the same as for $L=200$, as can be seen in Table I for the continuous transitions, suggesting that the latter are already quite close to their limiting (infinite-L) values.

The two methods yield slightly different predictions for the continuous transition line. Method A is more robust since we use data near the maximum-current value to perform the fit of the current-density relation, while in method B, data from this region are not included and the position of the maximum is rather sensitive to one's choice of the range of values fit using the polynomial. Indeed, the behavior of the

TABLE I. Values of α and β at the continuous transitions obtained via methods A and B.

	Method A		Method B	
L	α_c	β_c	α_c	β_c
100	1.034(3)	0.723(1)	0.9292(6)	0.6903(2)
200	0.966(2)	0.717(1)	0.941(1)	0.6970(2)
500	0.958(2)	0.725(1)	0.9413(7)	0.6957(2)

phases boundaries outside the fitting region (i.e., for $\alpha > 0.85$ or $\beta > 0.6$) is somewhat dependent of the choice of fitting region in both methods, since the mapping from (ρ_-, ρ_+) to (α, β) employs an extrapolation of the data for $\rho_-(\alpha)$ and $\rho_+(\beta)$ outside the fitting region.

While the continuous-space phase diagram is isomorphic to that of the lattice model, there are some differences between the two cases that appear likely to persist in the infinite-size limit. Since the lattice model possesses particle-hole symmetry, the phase diagram is invariant under the exchange of α and β. Thus, the boundary between the high- and low-density phases is a straight line extending from the origin to the point (1/2,1/2) in the α-β plane. The phase diagram of the continuous-space model does not possess this symmetry; the phase boundary between the high- and low-density phases does not fall along the line $\alpha=\beta$ and appears to be somewhat curved.

One might inquire whether the differences in the phase boundaries of the lattice and continuous-space models merely reflect finite-size effects in the latter. We have verified that in the *lattice* TASEP with $L=200$, the phase boundaries fall quite near their expected (infinite-size) positions. Comparison of the phase boundaries (in continuous space) for $L=200$ and 500 suggests that finite-size effects are somewhat stronger in the continuous-space model than on the lattice. Given the lack of particle-hole symmetry, however, it appears very unlikely that the continuous-space phase boundaries will converge to those of the lattice model in the infinite-size limit. One might argue that the curvature of our discontinuous transition line is a consequence of extrapoling the polynomial fit to regions out of the fitting region $\alpha < 0.85$ and $\beta < 0.6$. But, as Fig. 9 shows, the curvature is already present for α and β values inside the fitting region.

The differences between the lattice and continuous-space models reflect, in part, the absence of particle-hole symmetry in the latter; particle positions fluctuate in continuous space, but are fixed in the lattice model. In continuous space, moreover, particles occupying neighboring wells may influence one another via the repulsive potential V_{int}. On the lattice no such influence exists beyond simple exclusion. In continuous space, repulsive interactions should tend to spread particles more uniformly than on the lattice, promoting particle removal and hindering insertion. Thus, the transition from high to low density occurs for $\beta < \alpha$. Since repulsion is more significant for higher densities (i.e., larger α) the phase boundary should curve toward the α axis, as observed. The smaller value of β at the continuous transition [approximately 0.725(1) for $L=500$] compared to that of α [about 0.958(2) for $L=500$] may also be attributed to repulsion between neighboring particles.

B. Current: Comparison with mean-field theory

The absence of particle-hole symmetry is again evident in the current-density relation. In the lattice model, mean-field theory gives $J=\rho(1-\rho)$ [27,28], which is exact. Figure 10 compares the current on lattice with our results for continuous space. (Note that the latter exhibit virtually no finite-size effects on the scale of the figure.) Unlike in the lattice TASEP, here the current is not symmetric about $\rho=1/2$; it takes its maximum value at a density of about 0.57. The fact that the maximum current occurs at a higher density than on the lattice may again be attributed to interparticle repulsion.

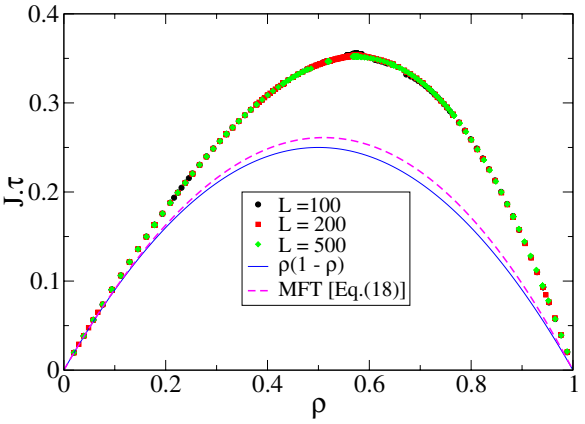

FIG. 10. (Color online) Current versus density in the lattice model (exact) and the continuous-space model.

On the lattice, the current is equal to the probability of having an occupied site with its neighbor on the right vacant, i.e., $J=\langle \xi_i(1-\xi_{i+1})\rangle$, $\forall i$, where ξ_i is an indicator variable equal to 1 if site i is occupied and zero if it is empty. In mean-field theory the joint probability is factored, so $\langle \xi_i(1-\xi_{i+1})\rangle = \langle \xi_i\rangle\langle(1-\xi_{i+1})\rangle$, and setting $\langle \xi_i\rangle=\rho$ in the bulk, we obtain $J=\rho(1-\rho)$.

Since the rate for hopping to the well to the right is $1/\tau$, the above mean-field argument yields $J=\rho(1-\rho)/\tau$ when applied to the continuous-space model. Figure 10 shows that this is in poor agreement with simulation. The mean-field analysis can go wrong in at least two respects: the jump rate may be modified by the presence of particles in neighboring well, and the factorization of the joint probability distribution may not be valid. Consider first the influence of neighbors on the jump rate. Due to repulsive interactions between neighboring particles, a particle in well $i-1$ affects the rate of hopping from i to $i+1$. As a first approximation we write

$$J = P(0,1,0)j(0,1,0) + P(1,1,0)j(1,1,0), \tag{18}$$

where $P(\xi_{i-1},\xi_i,\xi_{i+1})$ is the joint probability for three adjacent wells and $j(\xi_{i-1},\xi_i,\xi_{i+1})$ is the transition rate in this configuration. Factorizing the joint probability, we have $P(0,1,0)=\rho(1-\rho)^2$ and $P(1,1,0)=\rho^2(1-\rho)$. It remains to evaluate the currents $j(0,1,0)$ and $j(1,1,0)$.

Consider $j(0,1,0)$, the rate to overcome the barrier between wells i and $i+1$, given that both $i-1$ and $i+1$ are empty. The mean first-passage time τ_{ca}, for a particle to overcome the barrier, is readily found via the analysis of the one-dimensional Fokker-Planck equation. From the standard result [29] we have

$$\tau_{ca} = \frac{1}{k_B T}\int_a^c e^{U(x')/k_BT}dx' \int_{-\infty}^{x'} e^{-U(x'')/k_BT}dx'', \tag{19}$$

where $a=x_0$ and $c=x_0+2d_0$ are the positions of adjacent potential minima, with x_0 given by Eq. (13). Using the effective external potential [Eq. (11)] for $U(x)$ (since there are no in-

teractions with other particles), numerical evaluation of Eq. (19) yields $\tau_{ca}=6.538$ s$=1/j(0,1,0)$. This value agrees to within uncertainty with our simulation result for the mean time τ for a particle to hop between adjacent wells when there are no other particles in the system. Thus, the mean-field curve in Fig. 10 agrees with simulation in the low-density limit.

To estimate the transition rate $j(1,1,0)$, we perform a Monte Carlo simulation to determine the mean time required for a particle to hop to the next well, when the preceding well is occupied, and there are no other particles in the system. This yields $1/j(1,1,0)=5.548$ s. Although the presence of the trailing particle leads to an increase of about 18% in j, the effect is not sufficient to yield quantitative agreement with the current observed at higher densities (Fig. 10). Note however that at moderate and high densities, strings of $n \geq 3$ occupied wells occur with finite probability, and the cumulative effect of repulsions along the chain should make the hopping rate of the lead particle an increasing function of n. Simulations of $n=3-9$ occupied wells show that the transition rate of the first particle grows with n, but not enough to account for the value of the current observed in simulation.

We have also verified that the mean-field factorizations $P(0,1,0)=\rho(1-\rho)^2$ and $P(1,1,0)=\rho^2(1-\rho)$ are not very accurate in the continuous-space model. For density $\rho \simeq 0.52$, for example, we find

$$\frac{P(0,1,0)}{\rho(1-\rho)^2} \simeq 1.21, \tag{20}$$

$$\frac{P(0,1,1)}{\rho^2(1-\rho)} \simeq 1.04, \tag{21}$$

implying a significant correction to the mean-field theory predictions. We defer the development of a quantitative theory for $J(\rho)$ to future work.

C. Fluctuations

To close this section we note an interesting finding on fluctuations. The variance of the density, as a function of α, with fixed β, exhibits a maximum at the discontinuous transition (see Fig. 11). For β values such that the transition is continuous, by contrast, no peak in var(ρ) is observed at the transition. (Similar behavior is found, varying β with α fixed.) The large density fluctuations are associated with the presence of a shock separating high- and low-density regions, whose position fluctuates over the entire system. The position of maximum variance agrees to within uncertainty with the lines of the (discontinuous) phase transitions reported in Fig. 9. While the total energy exhibits fluctuations similar to those observed in the density, we do not find any signal in var(J) associated with the phase transitions.

V. DISCUSSION

We propose a continuous-space model of interacting Brownian particles in a periodic potential as a possible realization of the TASEP. The particles are subject to a constant drive in a periodic external potential. Using numerical integration of the Langevin equation and Monte Carlo simulation, we study systems of $L=100$, 200, and 500 wells. Our results show that the continuous-space model exhibits continuous and discontinuous phase transitions analogous to those observed in the lattice TASEP. The phase diagram of the continuous-space model is similar to that of the lattice model, but exhibits some differences due to the absence of particle-hole symmetry. This difference appears to be associated with fluctuations of particle positions around potential minima. Such fluctuations, together with the repulsive interactions between neighboring particles, cause the current to attain its maximum value at a density somewhat greater than 1/2, the density marking the maximum current in the lattice model. We expect these changes (relative to the lattice model) to be generic for continuous-space systems exhibiting TASEP-like phase transitions.

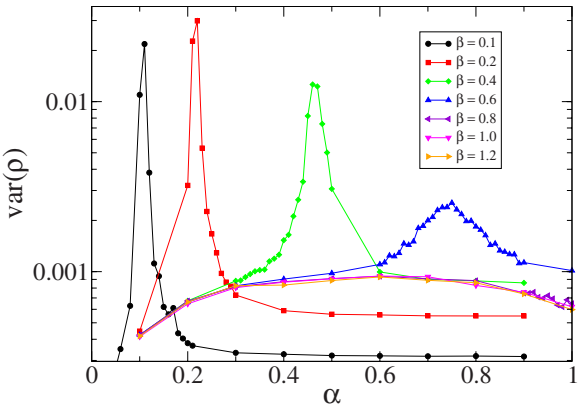

FIG. 11. (Color online) Density variance versus α for β values as indicated. System size $L=200$.

We believe that the present study demonstrates the possibility of observing TASEP-like behavior in laboratory experiments on systems of interacting colloidal particles in a one-dimensional optical tweezers array. The essential features of the TASEP—localization of particles in potential wells, with multiple occupancies prohibited, and biased hopping along the line—are readily accomplished with an appropriate choice of particle, fluid, and tweezers array parameters. It is however less obvious how to implement random insertion and removal of particles at the first and last wells of the array. Particle manipulation can be accomplished using optical tweezers to transfer particles between wells and reservoirs. To transfer particles in a random fashion, these tweezers would have to be intrinsically noisy or chaotic, controlled by a random number generator or driven by a noise signal. A simpler alternative may be *periodic* insertion and removal. In this case, one inserts a particle into the first well (when empty) at intervals of τ/α and checks for occupancy of the final well at intervals of τ/β, removing the particle if the well is occupied.

A preliminary study of the continuous-space model using periodic insertion and removal confirms that the three TASEP phases are again found. The density profiles under periodic and random particle transfer are very similar in the maximum-current phase, where the density profile is insensitive to small changes in the insertion and removal rates. Small systematic differences do however appear in the other phases, as shown in Fig. 12.

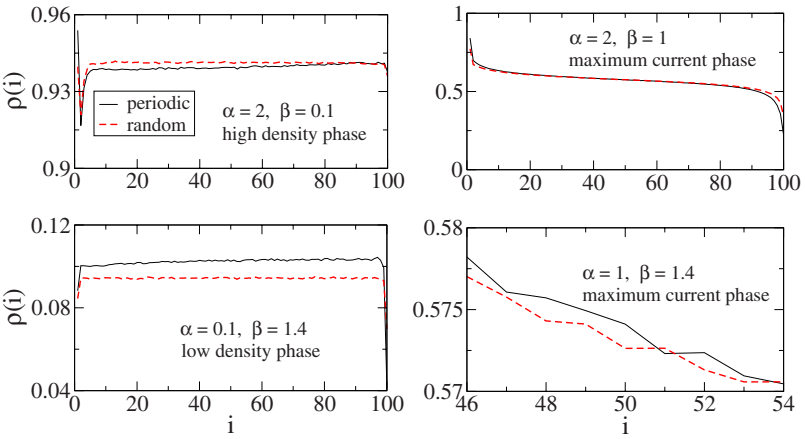

FIG. 12. (Color online) Comparison of density profiles obtained using periodic (black solid curve) and random (red dashed curve) insertion and removal; $L=100$.

Although our study strongly suggests the feasibility of a laboratory realization of the TASEP, a number of additional features would have to be included in the model before a quantitative comparison with experiment could be made. The principal modifications we expect to be necessary are study of a three-dimensional model, allowing fluctuations in directions perpendicular to the array axis, and inclusion of hydrodynamic interactions between the particles. We defer these tasks to future work.

ACKNOWLEDGMENTS

We thank O. N. Mesquita, U. Agero, and J. G. Moreira for helpful comments. This work was supported by CNPq and Fapemig, Brazil.

[1] B. Schmittmann and R. K. P. Zia, in *Phase Transitions and Critical Phenomena*, edited by C. Domb and J. L. Lebowitz (Academic, London, 1995), Vol. 17; Phys. Rep. **301**, 45 (1998).
[2] J. Marro and R. Dickman, *Nonequilibrium Phase Transition in Lattice Models* (Cambridge University Press, Cambridge, England, 1999).
[3] S. Katz, J. L. Lebowitz, and H. Spohn, Phys. Rev. B **28**, 1655 (1983).
[4] K.-t. Leung, B. Schmittmann, and R. K. P. Zia, Phys. Rev. Lett. **62**, 1772 (1989).
[5] J. T. MacDonald, J. H. Gibbs, and A. C. Pipkin, Biopolymers **6**, 1 (1968).
[6] E. D. Andjel, M. Bramson, and T. M. Liggett, Probab. Theory Relat. Fields **78**, 231 (1988).
[7] T. E. Harris, J. Appl. Probab. **2**, 323 (1965).
[8] F. Spitzer, Adv. Math. **5**, 246 (1970).
[9] J. T. MacDonald and J. H. Gibbs, Biopolymers **7**, 707 (1969).
[10] K. Heckmann, in *Passive Permeability of Cell Membranes*, edited by F. Kreuzer and J. F. G. Slegers (Plenum, New York, 1972), Vol. 3, p. 127.
[11] A. Schadschneider, Physica A **285**, 101 (2000).
[12] G. von Heijne, C. Blomberg, and H. Liljenström, J. Theor. Biol. **125**, 1 (1987).
[13] V. Kukla, J. Kornatowski, D. Demuth, I. Girnus, H. Pfeifer, L. Rees, S. Schunk, K. Unger, and J. Kärger, Science **272**, 702 (1996).
[14] T. M. Liggett, *Interacting Particle Systems* (Springer-Verlag, New York, 1985); *Stochastic Interacting Systems: Contact, Voter and Exclusion Process* (Springer-Verlag, Berlin, 1999).
[15] H. Spohn, *Large Scale Dynamics of Interacting Particles* (Springer, New York, 1991).
[16] G. Schütz and E. Domany, J. Stat. Phys. **72**, 277 (1993).
[17] B. Derrida, M. R. Evans, V. Hakim, and V. Pasquier, J. Phys. A **26**, 1493 (1993).
[18] B. Derrida and M. R. Evans, *The Asymmetric Exclusion Model: Exact Results Through a Matrix Approach in Nonequilibrium Statistical Mechanics in One Dimension* (Cambridge University Press, Cambridge, England, 1996).
[19] B. Derrida, Phys. Rep. **301**, 65 (1998).
[20] J. M. Sancho, A. M. Lacasta, K. Lindenberg, I. M. Sokolov, and A. H. Romero, Phys. Rev. Lett. **92**, 250601 (2004).
[21] P. T. Korda, M. B. Taylor, and D. G. Grier, Phys. Rev. Lett. **89**, 128301 (2002).
[22] M. P. MacDonald, G. C. Spalding, and K. Dholakia, Nature (London) **426**, 421 (2003).
[23] P. Y. Chiou, A. T. Ohta, and M. C. Wu, Nature (London) **436**, 370 (2005).
[24] A. M. Lacasta, J. M. Sancho, A. H. Romero, and K. Lindenberg, Phys. Rev. Lett. **94**, 160601 (2005).
[25] Y. Roichman, V. Wong, and D. G. Grier, Phys. Rev. E **75**, 011407 (2007).
[26] A. B. Kolomeisky, G. M. Schütz, E. B. Kolomeisky, and J. P. Straley, J. Phys. A **31**, 6911 (1998).
[27] J. Krug, Phys. Rev. Lett. **67**, 1882 (1991).
[28] B. Derrida, E. Domany, and D. Mukamel, J. Stat. Phys. **69**, 667 (1992).
[29] N. G. van Kampen, *Stochastic Processes in Physics and Chemistry* (Elsevier, Amsterdam, 2007).